Design and Analysis of the Thermal Management System of a Hybrid Turboelectric Regional Jet for the NASA ULI Program

Mingxuan Shi[1], Mitchell Sanders[2], Alan Alahmad[3], Christopher Perullo[4], Gokcin Cinar[5], and Dimitri N. Mavris[6]

Aerospace Systems Design Laboratory, School of Aerospace Engineering, Georgia Institute of Technology, Atlanta, Georgia, 30332

A team of researchers from multiple universities are collaborating on the demonstration of a hybrid turboelectric regional jet for 2030 under the NASA ULI Program. The thermal management is one of the major challenges for the development of such an electric propulsion concept. Existing studies hardly modeled the thermal management systems with the propulsion systems nor integrated it to the aircraft for system- and mission-level analyses. Therefore, it is very difficult to verify whether a design of the thermal management system is feasible and optimal based on current literature. To fill this gap, this paper presents a design of the thermal management system for the hybrid turboelectric regional jet under the ULI program and integrates it to the aircraft. The TMS is tested against the cooling requirements, where the thermal loads from the electric propulsion system are quantified through the whole mission. Potential solutions for peak thermal loads during takeoff and climb are also proposed and analyzed, where additional coolant or phase change materials are used. Moreover, the impacts of the TMS on the system- and mission-level performance are investigated by the presented integration approach as well. It is discovered that a basic oil-air thermal management system cannot fully remove the heat during the early mission segments. Using additional coolant or phase change materials as heat absorption can handle such heating problem, but penalty due to additional weight is added. It is found that greater penalties in fuel burn and takeoff weight are added by additional coolant solution than the phase change material solution.

I. Introduction

Significant improvement of technologies is needed to meet emerging aggressive environmental and fuel economy goals. The National Aeronautics and Space Administration (NASA) N+3 [1] aims to achieve a reduction of emissions higher than 75%, and a reduction of aircraft fuel burn higher than 70%. Similarly, European Clean Sky [2] sets the target on the reduction of the emissions and the noise, where the goals are to reduce CO_2, NO_x, and noise by 75%,

---

[1] Graduate Research Assistant, ASDL, School of Aerospace Engineering, Georgia Tech, AIAA Student Member
[2] Graduate Research Assistant, ASDL, School of Aerospace Engineering, Georgia Tech
[3] Graduate Research Assistant, ASDL, School of Aerospace Engineering, Georgia Tech
[4] Senior Research Engineer, ASDL, School of Aerospace Engineering, AIAA Member
[5] Research Engineer II, ASDL, School of Aerospace Engineering, AIAA Member
[6] S.P. Langley Distinguished Regents Professor and Director of ASDL, Georgia Tech, AIAA Fellow

90%, and 65% by 2050 respectively. A number of technologies and aircraft concepts have been proposed and studied to meet such goals, and the turboelectric aircraft is one of the concepts of interest. Under the NASA University Leadership Initiative (ULI) program, teams from The Ohio State University (OSU), Georgia Tech (GT), University of Wisconsin-Madison (UW), University of Maryland (UMD), and North Carolina A&T (NCA&T) are collaborating to demonstrate the concept of Hybrid Turboelectric Distributed Propulsion (HTeDP) with corresponding technologies for a 2030 regional jet, of which the previous work has been summarized in authors' previous paper [3] and the update is summarized in the accompanying paper this year [4].

One of the major challenges in such electric propulsion concepts is the thermal management of the overall electric systems. Most of the produced heat in the conventional propulsion system is in the exhaust air which can be easily disposed. In contrast, the heat generated by the electric propulsion system is not in the form of the exhaust, making the heat removal more challenging. On the other hand, the heat generated by the electric propulsion system is much larger than the heat generated by other existing electric systems in the aircraft. Considering the class of a reginal jet as studied in NASA ULI program, each motor is of 2.1 MW (8 in total) with a corresponding efficiency around 0.98 [3]. The corresponding heat generated is around 42 kW (336 kW in total), which is significantly larger than current electric systems applied in the aircraft. Therefore, the existing cooling approaches for electric systems may not be suitable anymore, and thus a new thermal management system (TMS) is in need for the turboelectric concept. It should be notified that the general TMS in an aircraft should include the subsystems which remove any waste heat generated all over the aircraft, such as the environmental control systems (ECS) to cool the cabin, cooling systems to cool the battery, and subsystems to cool the propulsion systems. However, the TMS of interest in this paper only refers to the subsystem that removes the heat generated from the electric propulsion system where the major cooling challenges lie in. Since the conventional ECS is cable of cooling both the cabin and the battery as shown in the previous work [3], the corresponding TMS for these two systems will not be discussed in detail in this paper.

There have been a lot of studies on the turboelectric concept, however, most of them modeled the TMS of the electric propulsion system as only penalty coefficients in weight and power consumption, without an actual design and modeling of the TMS nor the integration of it to the aircraft for system- or mission-level analyses. For example, Felder [5, 6] proposed a design of a turboelectric distributed propulsion system (TeDP), and showed an analysis of the advantages of this concept. However, the electric systems, including generator, transmission systems, and motors, were assumed superconducting, and the corresponding TMS options were assumed to be cryocooler or liquid hydrogen cooling. Such TMS were considered only as part of the propulsion system with expected overall efficiency and weight, without the actual modeling and integration. Liu [7] conducted a research on thermal cycle analysis of TeDP system, and presented a TSFC benefit coming from the TeDP concept. Superconducting for the electric systems were assumed, but the impacts of TMS on the performance were not considered as well. Welstead [8] studied a turboelectric concept, STARC-ABL, where two under-wing turbofans (generators) power an electric propulsor at the tail, discussing the sizing and performance results for this concept. Similarly, the losses due to TMS were ignored, while the weight was only approximated based on the specific power from a More-Electric Aircraft (MEA) configuration. The authors' previous work (by Shi and Pokhrel [9-11]) has also performed modeling analyses on the TeDP configuration, while neglecting the penalties caused by the TMS. On the other hand, many researchers have studied the TMS for the electric propulsion systems, however, many of them only provided qualitative analysis or subsystem-level quantitative analysis, leaving the impacts of the TMS on the aircraft unknown. For example, McCluskey [12] discussed several potential cooling approaches while neglecting their aerospace applications. Kabir [13] investigated several thermal management options, only focusing on the heat transfer performance of the TMS, while leaving the impacts of the proposed TMS on the aircraft unknown. Rheaume [14] did analyze the TMS through a given mission for an aircraft. The analysis was done by incorporating thermal loads for typical mission segments as boundary conditions for the TMS model. However, the TMS was not integrated to the aircraft, and the aircraft performance was also neglected, making it possible to analyze the impacts of TMS at system or mission level.

From the review of the literature, there exists a gap that existing studies hardly considered the TMS in the analysis of the electric propulsion system nor investigated its impacts on the aircraft at system or mission level. Therefore, it can be difficult to verify whether a proposed TMS is even feasible in either handling the heat or applied in an aircraft in such a manner. An optimal design of the TMS cannot be determined as well. To fill this gap, this paper proposes a design of the TMS for an electric propulsion system of HTeDP aircraft, and further integrates it to the aircraft to perform mission-level study, through a modeling and integration environment, *Georgia Tech Hybrid Electric Analysis Tool* (GT-HEAT) [15]. The thermal loads requirements are examined through the whole mission, and potential solutions for the peak thermal load during takeoff and climb are also investigated. Moreover, the impacts of the TMS on the aircraft performance due to additional weight and power consumption are quantified in terms of the maximum takeoff weight (MTOW) and mission block fuel.

This paper organizes as follows: the architectures of the electric propulsion system, TMS, and potential solutions for the peak thermal load during takeoff and climb are discussed in Section II; the integration and modeling approaches are briefly introduced in Section III; Section IV illustrates the cases to run for this study, where the specifications of the aircraft and the selected mission profile are provided, as well as the metrics of interest; the results are then discussed in Section V; the conclusions and the future work are presented in Sec. VI.

II.   Architecture of the Thermal Management System

A. Architecture of the Electric Propulsion System

Before discussing the TMS architecture, the electric propulsion system to be cooled is briefly introduced here, as illustrated in Fig. 1. This architecture is consistent with the previous paper [3] and the update of the ULI program in this year [4], where more details can be found. As shown in this figure, the electric propulsors, which are the electric fans driven by the motors. The electrical power comes from two sources: one is the generator, which is driven by the turboshaft engine, another source is the battery. It should be noted that in the configuration selected in this paper, four electric propulsors (8 in total for the whole aircraft) are driven by one generator (two generators in total), and there is only one battery in the aircraft. A more detailed discussion of the aircraft configuration will be introduced in Section III. The propulsion architecture is presented in this way only for simplicity. As discussed before, the battery is cooled by the ECS, thus the corresponding cooling approaches for the battery will not be discussed in detail here. The TMS of interest in this context cools the electric propulsor, where the heating source includes the inverter and motor.
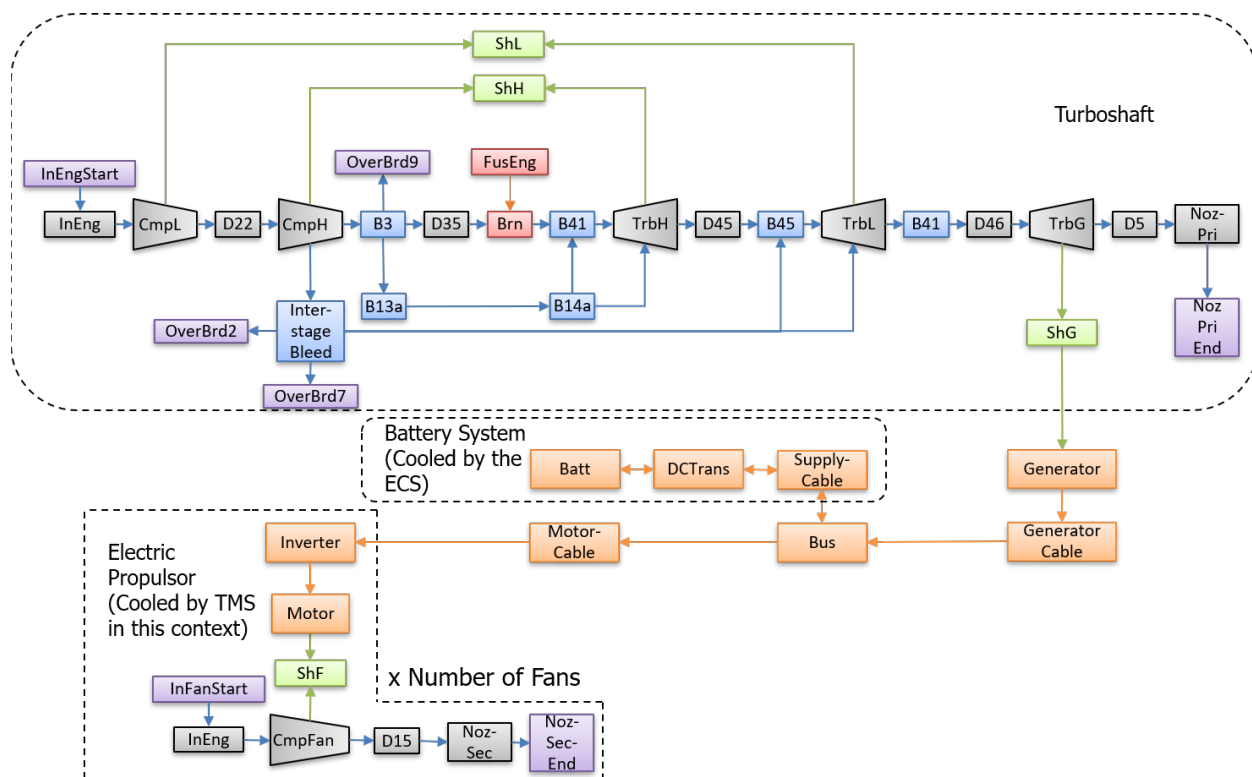

Fig. 1 Architecture of the overall propulsion system

B. Architecture of the TMS

The architecture of the TMS is presented in Fig. 2. The heat generated from the motor and inverter is dumped into the cooling oil through the integrated motor drive (IMD) heat exchanger (HX), where the oil is pumped from the reservoir. Polyalphaolefin (PAO) is selected as the cooling oil in this architecture. The corresponding entrance and exit temperatures of PAO through the IMD HX are determined by the other team under the ULI program. After cooling the motor and inverter in the IMD HX, the oil is then pumped to the air-cooled oil cooler (ACOC), where the oil is cooled to the required cooling temperature (55°C) by the bleed extracted from the electric fan. The amount of the extracted fan bleed is adjusted to cool the oil to its target temperature, constrained by a user specified bleed extraction

upper limit. Then the cooling oil loops back to the reservoir. The cooling fan bleed after passing through the ACOC mixes with the core steam of the fan, and then it is disposed through the nozzle as exhaust.
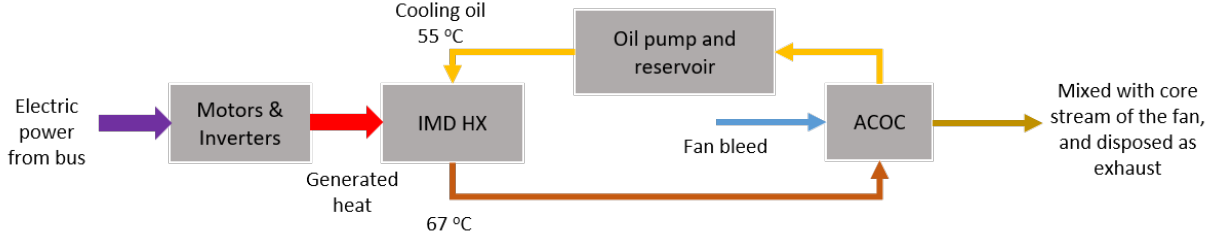

Fig. 2 Architecture of the TMS

However, the cooling capability of this TMS strongly depends on the air temperature which is determined by the flight conditions, and it is also constrained by the maximum amount of cooling bleed that can be extracted. During takeoff and climb, the thermal load is at the peak because the propulsion system needs to produce the maximum power in these conditions. Meanwhile, the cooling capability of the fan bleed air is the lowest due to high temperature at low altitude. Therefore, there exists a potential problem that this TMS may not be able to remove all the heat generated from the inverter and the motor during takeoff and climb, even if its capability satisfies the cooling requirements in other mission segments such as cruise and descent. Thus, solutions to handle the peak thermal load during takeoff and climb may be needed, which will be discussed in Sec. II. C.

This TMS influences the system-level and mission-level performances in following ways: an additional pressure drop is added to the fan flow which reduces the effective thrust; and penalty weights are also added to the system because of the ACOC heat exchanger, the coolant, and the corresponding pipes and reservoirs. The pressure drop is generated as part of the fan bleed is extracted to cool the PAO and then is mixed back into the core flow stream. The pressure drop to the fan flow, the ACOC heat exchanger weight, and the PAO weight in the heat exchanger are calculated using the ACOC heat exchanger model, which was constructed in the previous work [21] based on the ε-NTU method [20]. An introduction of the modeling method will be briefly discussed in Sec. III. B. 1. The PAO weight in the IMD is estimated using the coolant volume data provided by the ULI team from University of Maryland. The coolant volume is 6.5 litters for a 1-MW IMD. It should be noted that a full-size ULI aircraft requires 2.1-MW IMD, and the current 1-MW IMD is only developed for validation of the motor technologies. Therefore, a 2.1-MW IMD should be used for the assessment of the TMS because this paper presents the analysis of the TMS integrated to the full-size ULI aircraft. By assuming the same volume-specific power of the IMD, the coolant volume is simply scaled by the ratio of 2.1/1. Then the weight of the PAO can be obtained using the scaled volume. Another scalar, 2, is also multiplied to the coolant weight to estimate the weights of the PAO reservoir and pipes.

C. Potential Solutions for Peak Thermal Load during Takeoff and Climb

Two potential solutions are proposed in this paper: (1) Use additional PAO to absorb the heat that cannot be removed; (2) Use phase change material (PCM) to absorb the heat that cannot be removed. The impacts of these two methods are also compared and discussed in Section. V.

1. PAO to Absorb the Heat

The architecture to use additional PAO to absorb the heat is shown in Fig. 3. There are two oil reservoirs: one for the cold oil in which the oil temperature is 55°C, and another in the hot oil reservoir which is to contain hot oil that is not cooled through the ACOC. Only cold oil is supplied to the IMD HX to cool the motor and inverter. Then the portion that can be fully cooled by the fan bleed is fed to ACOC for cooling, and it is further sent back to the cold oil. The portion that cannot be cooled is then directly sent to the hot oil reservoir. In such a manner, the additional weight due to additional PAO is minimized, since the temperature rise of the additional PAO is maximized which is from 55°C to 67°C. The impact of this solution is that penalty weight is added to the system due to additional PAO. The mass of the additional PAO is given by the following equation, where $m_{PAO,add}$ is the mass of the additional PAO, Q_{excess} is the generated heat that cannot be removed, $T_{IMD,in}$ is the PAO temperature when entering IMD which is 55°C, $T_{IMD,out}$ is the PAO temperature when exiting IMD which is 67°C, and $c_{p,PAO}$ is the specific heat capacity of PAO:

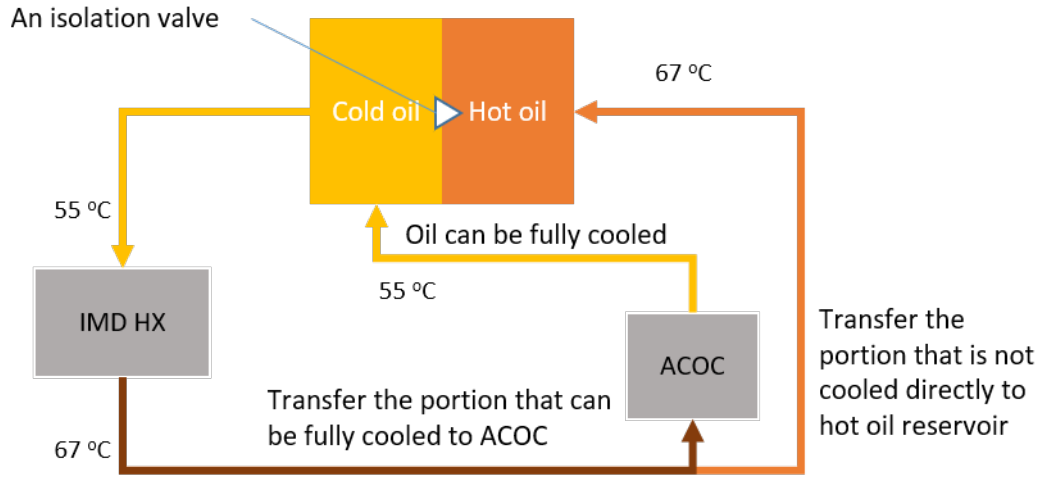$$m_{PAO,add} = \frac{Q_{excess}}{\int_{T_{IMD,in}}^{T_{IMD,out}} c_{p,PAO}(T)dT} \tag{1}$$

Fig. 3 Architecture incorporating additional PAO for heat absorption during takeoff and climb

2. PCM to Absorb the Heat

Another option is to use PCM to absorb the heat instead of using the PAO. The advantage of applying PCM is that the expected additional weight can be much smaller than using PAO, because of their high specific latent heat (latent heat/weight ratio). The proper PCM should be selected in terms of the working temperature of the motor and the inverter. The working conditions for the IMD were provided by the team from University of Wisconsin-Madison [3]: the target working temperature of the stator is 135°C, and the its maximum working temperature is 180°C; the target working temperature of the rotor is 139°C, and its maximum working temperature is 200°C. Based on such working conditions, two types of PCM, magnesium chloride hexahydrate (salt hydrate) [23] and Urea-KCl (eutectic compound) [24], are selected for assessment, and the corresponding properties are listed in Table 1. It should be noted that the melting temperatures of the selected PCM are both slightly lower than the target working temperature to effectively remove the heat when the IMD is working at its optimal operation temperature.

Table 1 Properties of the selected PCM

PCM Name	Melting Point (°C)	Latent Heat (kJ/kg)	Specific Heat (kJ/(kg.K))		Thermal Conductivity (W/ (m.K))		Density (kg/m³)	Refs
			Solid	Liquid	Solid	Liquid		
magnesium chloride hexahydrate	117	150	2.0	2.4	0.70	0.58	1570	[23]
Urea-KCl	115	227	1.69	1.96	0.830	0.660	1370	[24]

The architecture to incorporate PCM to store heat generated by the IMD is shown in Fig. 4. It should be noted that the purpose of this figure is only to illustrate the heat removal directions, and the IMD dimensions are not in proportion to the dimensions in reality, and flow path of the PAO is much more complicated. The real dimensions of the IMD are: diameter = 254 mm, and height = 186 mm. As presented in other ULI papers [3,4], the IMD is an inner rotor motor. Therefore, the PCM can be attached to the external surface of the stator. The coolant, PAO, still passes through the cooling jacket inside the IMD as the original motor design, to which part of the generated heat is dumped ($\dot{Q}_{PAO}$). The PCM shell directly absorbs the heat from the stator ($\dot{Q}_{PCM}$). The detailed heat transfer analysis and sizing of the PCM along with the simplifying assumptions are discussed in Sec. III. B. 2, where a 1-D PCM model is incorporated. It should be noted that many detailed geometric features of the IMD are neglected, and many assumptions are made to simply the heat transfer analysis. However, this paper focuses on a high-level analysis of the influences of different TMS architectures on the system-level and mission-level performances to support the TMS design decision making. Therefore, such low-fidelity modeling of the PCM is reasonable because it is sufficient to represent the characteristics

5

of the PCM as well as to reduce the computational cost. If more detailed design of the TMS is needed in the future, higher-fidelity approaches can be then introduced.
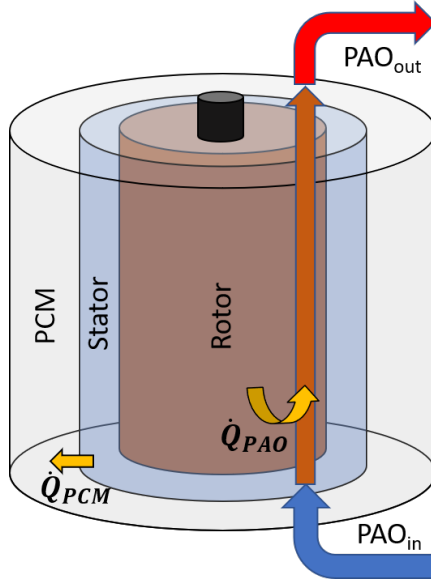

Fig. 4 Architecture incorporating PCM for heat absorption during takeoff and climb

III.   Integration Environment (GT-HEAT) and Modeling Methodology

A. GT-HEAT

The modeling and integration in this paper is done in the *Georgia Tech Hybrid Electric Analysis Tool* (GT-HEAT) [15]. A detailed description can be found in Perullo and Gladin's work [15, 17, 18], while only the fundamental idea of this toolset is briefly introduced in this section. This environment allows the analysis modules of the engine, vehicle and the mission to exchange full state information at each operation state (or each mission point). As illustrates in Fig. 5, the overall aircraft mission analysis is represented by a mission assembly, an airframe assembly, and an engine assembly. The TMS in GT-HEAT is modeled in the engine assembly, which influences the engine performance through power and bleed extraction. The TMS model also updates the weight to the aircraft assembly. The modeling environment in GT-HEAT is the Numerical Propulsion System Simulation (NPSS) [19], because NPSS is the industry standard propulsion modeling software and it also has the zooming capability as well as the function to create both open source and compiled, proprietary modules. The NPSS not only models the propulsion system but also the power distribution systems, electrical systems, thermal management systems, and energy storages.

The mission analysis process of GT-HEAT works clockwise, as shown in Fig. 5. Staring from the mission assembly, a user defined mission profile provides the flight conditions of the current mission segment to the airframe assembly. Receiving the operation conditions, the airframe assembly computes the required states to realize this flight condition, such as the required thrust, weight, temperatures of the fuel tank and the cabin, and electric power requirements. Then such required states are fed to the engine assembly, and the engine assembly computes the engine performance using maps or analysis tool with selected fidelities. Then the outputs are sent back to the mission assembly to check if the computed solutions converge with the initial guesses for the mission. The computed fuel flow is also updated to the airframe assembly, which influences the weight.
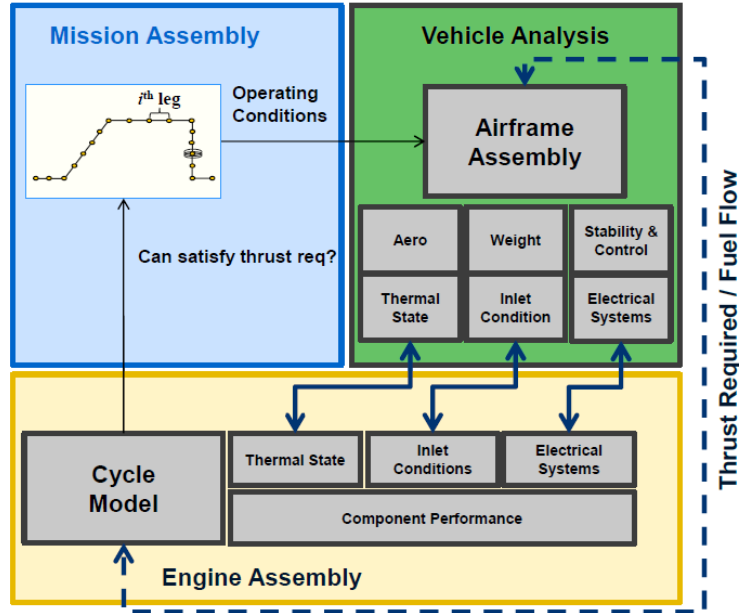
Fig. 5 GT-HEAT functional architecture

B. Modeling Methodology

1. TMS Modeling Methodology

The modeling methodology is briefly introduced in this section, since some details have been discussed in the previous paper [3]. Most of the components modeled in the TMS, as shown in Fig. 2, are standard NPSS elements, which are modeled in a 0-D manner by using performance parameters, and the such performance parameters are looked up from off-design maps. The components modeling by such 0-D approach are duct, compressor (fan), turbine, shaft, motor, inverter, nozzle. The IMD HX is not actually modeled in the TMS. However, its performance is estimated by the relation of the mass flow of the oil and the entrance and exit temperatures, which are given by the team of University of Wisconsin-Madison. The maps of turbomachines (compressor and turbine) are obtained by scaling typical maps of a compressor and a turbine of a similar application. The maps of the motor and inverter are also given by the team of University of Wisconsin-Madison. The air/oil heat exchanger (ACOC) is modeled using the ε-NTU relation, following the approach in Kays and London's book [20]. The detailed implementation can be found in Shi's previous paper [21].

2. PCM Modeling Methodology

A 1-D model is applied to analyze the heat transfer from the stator to the PCM as well as the phase change process. This method is based on the work done by Mansouri [25], where the phase change problem was formulated as a Stephan problem and an analytical solution of Neumann was applied to solve the problem. In the 1-D domain, the simplification of the stator-PCM heat transfer geometric configuration is illustrated in Fig. 6. At x=0, the external surface of the stator is attached to the PCM inner surface, where the heat is transferred from the stator to the PCM. The liquid-solid interface is at $x=X_f$, where the melting process happens. When $0<x<X_f$, the PCM is of the liquid state. When $X_f<x$, the PCM is of the solid state, where this formulation takes the PCM as a semi-infinite medium from x=0 to infinity. It should be also noted that such formulation is based on the melting process of a pure material. However, to simplify the computation, this paper assumes that the PCM of interest follow the behaviors of a pure material. Another assumption in this formulation is that the convection in the liquid section of the PCM is ignored. The radiation is not considered either. Thus, the heat transfer in this problem is only through conduction based on this assumption.
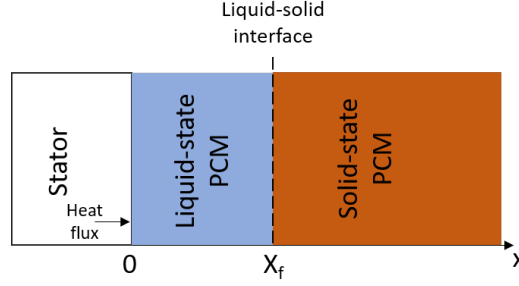
Fig. 6 1-D melting process of the PCM

The formulated governing equations, initial conditions, and boundary conditions are presented below, of which the detailed derivation process can be found in Mansouri's paper [25]. Some notations in the formulation are introduced here: the subscripts l and s indicate the liquid or solid state of the PCM; T refers to the temperature; k is the thermal conductivity; t is time; L is the latent heat; Cp is the specific heat capacity; T_{wall} is the temperature of the stator external surface; T_{melt} is the melting temperature; and T_0 is the initial temperature of the PCM.

Governing equation:

$$\frac{\partial T_l}{\partial t} = \frac{\partial}{\partial x}\left(\alpha_l \frac{\partial T_l}{\partial x}\right), 0 < x < X_f, t > 0 \ liquid\ phase \tag{2}$$

$$\frac{\partial T_s}{\partial t} = \frac{\partial}{\partial x}\left(\alpha_s \frac{\partial T_s}{\partial x}\right), X_f < x, \ t > 0 \ solid\ phase \tag{3}$$

where $\alpha = \frac{k}{\rho c_p}$ which is the PCM thermal diffusivity.

And the heat flux from the stator to the PCM can be expressed by:

$$q = \rho_l L \frac{\partial X_f}{\partial t} = k_s \frac{\partial T_s(X_f, t)}{\partial x} - k_l \frac{\partial T_l(X_f, t)}{\partial x}, t > 0 \tag{4}$$

Initial conditions at t=0:

$$T_s(x, 0) = T_0, \qquad 0 \le x \le R_{PCM}, \tag{5}$$

$$X_f(0) = 0 \tag{6}$$

Boundary conditions at t>0:

$$T_l(x = 0, t) = T_{wall} \tag{7}$$

$$T_l(x = X_f, t) = T_s(x = X_f, t) = T_{melt} \tag{8}$$

$$T_s(x \to \infty, t) = T_0 \tag{9}$$

One assumption is made here that the IMD is always working in its target working temperature because the PCM should be sized to absorb all the heat that cannot be removed by PAO, that is, the working temperature of the IMD will not change during the operation.

The analytical solution for this problem is given by the following equations:

$$\frac{T_l(x, t) - T_{wall}}{T_{melt} - T_{wall}} = \frac{\text{erf}\left(\frac{x}{2\sqrt{\alpha_l t}}\right)}{\text{erf}(\xi)}, 0 < x < X_f, t > 0, liquid\ phase \tag{10}$$

$$\frac{T_s(x, t) - T_0}{T_{melt} - T_0} = \frac{\text{erfc}\left(\frac{x}{2\sqrt{\alpha_s t}}\right)}{\text{erfc}(\nu\xi)}, X_f < x, t > 0, solid\ phase \tag{11}$$

The position of the liquid-solid interface is given by:

8

$$X_f(t) = 2\xi\sqrt{\alpha_l t} \tag{12}$$

where ξ is implicitly given by:

$$\frac{St_l}{e^{\xi^2}erf(\xi)} - \frac{St_s}{\nu e^{\nu^2\xi^2}erfc(\nu\xi)} = \xi\sqrt{\Pi} \tag{13}$$

The notations used in the solutions above are introduced here. *erf* and *erfc* are the error function and the complementary error function, which can be approximated by polynomials [25]:

$$erf(x) = a_0 + a_1 x + a_2 x^2 + a_3 x^3 + a_4 x^4 + a_5 x^5 \tag{14}$$

$$erfc(x) = 1 - erf(x) \tag{15}$$

where $a_0 = -0.00401$, $a_1 = 1.18669$, $a_2 = -0.14559$, $a_3 = -0.33443$, $a_4 = 0.16069$, $a_5 = -0.02155$. St_l and St_s are the Stephan number, which are expressed as: $St_l = C_{p_l}(T_{wall} - T_{melt})/L$ and $St_s = C_{p_s}(T_{melt} - T_0)/L$. $\nu = \sqrt{\alpha_l/\alpha_s}$. ξ is a constant parameter that can be obtained by solving the implicit equation Eq. (13). In the current application, a Newton solver is used to solve for ξ.

Then the Eq. (12) is known with the calculated ξ, and the heat flux from the stator to the PCM is known by substituting Eq. (12) into Eq. (4). Then the heat transfer rate can be calculated by multiplying the heat flux q by the heat transfer area S, which is expressed as $S = \Pi D_{IMD} h_{IMD}$, where D_{IMD} is the diameter of the IMD, and h_{IMD} is the height of the IMD. As illustrated in Fig. 4, the PCM has the same height as the IMD, and it is of a ring shape shelling the IMD stator. The only value needed to determine the PCM size is the distance between the stator external surface and the PCM external surface. Such distance can be approximated by $X_f(t_{melt})$ where t_{melt} is the time when the generated heat can be fully removed by the coolant in the original TMS for the first time. Such approximation is reasonable because the excessive heat only appears during the early mission segments, which will be shown in the Sec. V where the heat removal performances are discussed. Then the volume of the PCM, V, can be given by

$$V = \Pi\left(\left(\frac{1}{2}D_{IMD} + Xf(t_{melt})\right)^2 - \left(\frac{1}{2}D_{IMD}\right)^2\right)h_{IMD} \tag{16}$$

Then the mass of the PCM, m_{PCM}, can be calculated by

$$m_{PCM} = \rho V \tag{17}$$

IV. Analysis Cases for This Study

In this section, the setup of cases of interest in this paper is introduced. The aircraft configuration and the corresponding design conditions are given first. The off-design mission selected for this study for the thermal and performance analysis is then described. Metrics of interest to evaluate the TMS are also presented, following which the cases of interest in this paper are discussed.

A. Aircraft Configuration and the Design Mission

As mentioned before, the aircraft configuration applied in this study is the one for the NASA ULI program, which is a hybrid turboelectric distributed propulsion system with two wing tip mounted turbo generators powering the eight electric propulsors, as shown in Fig. 7. A battery can also be potentially installed at the aircraft floor.
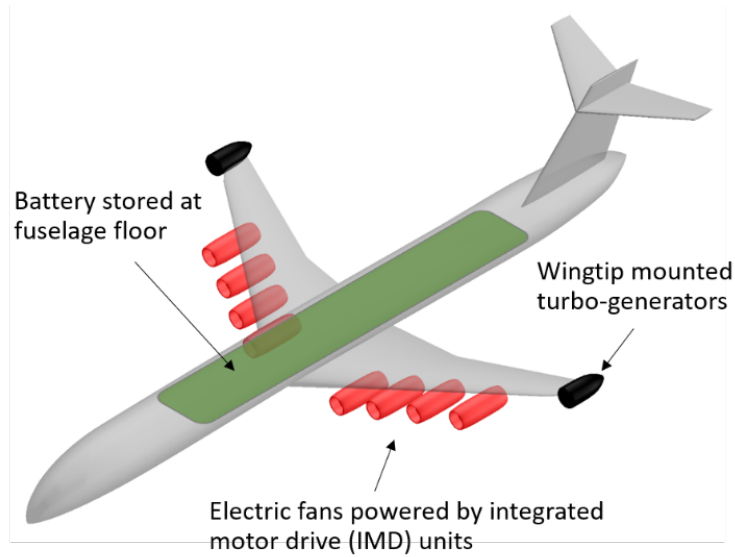
Fig. 7 Aircraft configuration for the NASA ULI program

As required by the ULI program [3], the aircraft should be sized without the installed battery through the design mission, while adding the battery to shorter-range off-design mission to study the benefits of hybridization. This means that during the design mission, all propulsive power is generated by the wingtip mounted turbo-generators, while during the shorter-range off-design mission the propulsive power is partially from battery and partially from the generators. The detailed optimization and sizing approaches for the aircraft and the battery can be found in the previous paper [3] and the updated metrics and sizing parameters can be found in Ref. [4], which will not be discussed in this paper. In this paper, only the parameters of the design mission are shown in Table 1, and the design mission profile is shown in Fig. 8, which are to give readers an idea of the class of the selected aircraft. It should be noted that a reserve mission is included in the design mission.

Table 2 Design information of the aircraft

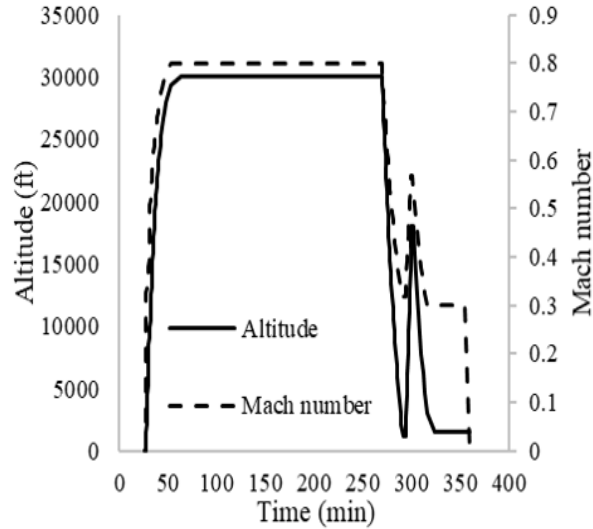| Parameters	Value
Passenger capacity	78
Design range, nmi	1,980
Design payload weight, lbm	18,060
Cruise Mach number	0.8
Maximum cruise altitude, ft	41,000
Maximum payload weight, lbm	23,350

Fig. 8 Design mission profile

B. Off-Design Missions for Analysis

The ULI program is focusing on improving the fuel burn performance by hybridizing aircraft, which introduces a battery as a power source for the mission. To satisfy the maximum takeoff weight (MTOW) constraint under the penalty by installation of the battery, the missions of interest for the ULI program are of relatively short ranges and low payloads [3, 4]. Therefore, only short-range and low-payload missions are selected for the study in this paper. For the thermal management analysis, the selected mission, as shown in Fig. 9, is of a 600-nmi range and an 8,100-lb payload, which are typical values for a regional jet [22]. The optimal battery usage profile during mission is that 17% power is supplied from the battery during climb and 23.5% power is supplied from the battery during cruise, which is obtained in the accompanying paper [4] that presents the updates in system assessment of the ULI aircraft in 2020. For the analysis of the TMS impacts on the fuel burn performance, off-design missions normalized ranges from 0.1 to 0.6 and normalized payloads from 0.1 to 0.6 are selected, where the range is normalized by the design range, 1,980 nmi, and the payload is normalized by the design payload, 18,060 lb.
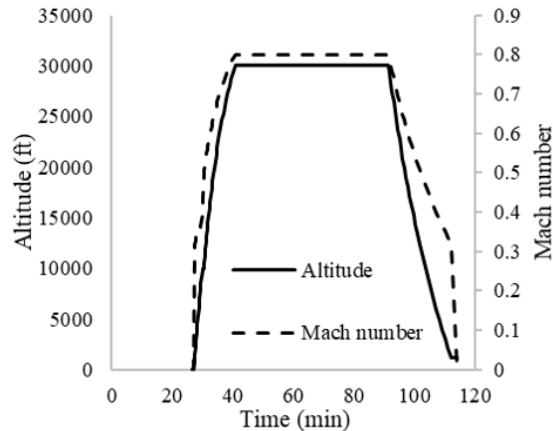

Fig. 9 Off-design mission profile

C. Metrics of Interest

To evaluate the thermal management capability of the TMS as well as its impacts on the aircraft and the mission, the following metrics are evaluated. Firstly, the heat removed from the motor and inverter is compared to the heat generated through the whole off-design mission. If the proposed TMS can remove all the heat generated, it is expected

that the removed heat should equal to the heat generation. However, if the heat generated cannot be fully removed during certain mission segments, it is expected that there exists a gap between the generated heat and the removed heat in these segments. The impacts of the TMS on the aircraft and mission are evaluated by the aircraft maximum takeoff weight (MTOW) and the mission block fuel when integrating the TMS to the aircraft. It is expected that the TMS can add more weight to the aircraft not only due to its own weight, but also because the engine needs to be upsized to account for the additional weight of the TMS and the power consumption of the TMS. The mission block fuel burn is also expected to increase, as both the weight and power consumption increase.

D. Cases of Interest

To investigate the capability of the TMS and its impacts on the aircraft, the following cases are analyzed in this study:

1. Baseline HTeDP Aircraft Neglecting TMS (Baseline)

The baseline HTeDP aircraft is sized and analyzed neglecting the TMS impacts, assuming all the heat can be removed without any penalty. This is a usual assumption that can be found in most existing literature, which does not account for the impacts of the TMS. An analysis of the heat generation from the IMD will be conducted using this baseline case to show the amount of heat that cannot be removed without TMS. This case also provides a baseline block fuel burn performance without TMS, which is to be compared with the performance considering the TMS to show its impacts.

2. An HTeDP Integrated with TMS without Solution for Peak Thermal Load (BaseTMS)

This case is to show the performance of the basic TMS without the solution for the potential peak load during early mission segments. This case is assessed to verify if the heat absorption solution for peak thermal load is needed. If the removed heat can be identified to be less than the generated heat, then such heat absorption solution needs further investigation. The mission block fuel burn performance influenced by the weight and power consumption penalties is also analyzed and compared to the baseline case.

3. An HTeDP Integrated with TMS with Additional PAO as the Solution for Peak Thermal Load (AddPAO)

This case uses additional PAO to absorb the heat that potentially cannot be removed by the basic TMS. A thermal management analysis is run to show the heat removal capability of this architecture. Additional weight will be also added to the aircraft due to additional PAO, so the block fuel burn analysis for this case considers the penalty weight as well as the upsizing effects.

4. An HTeDP Integrated with TMS with Salt Hydrate PCM as the Solution for Peak Thermal Load (PCM1)

This case incorporates a type of salt hydrate PCM, magnesium chloride hexahydrate, as the solution to absorb the heat that cannot be removed instead of using PAO. A thermal management analysis will be conducted to show the cooling capability of this type of PCM. The assessment of the block fuel burn performance for this case considers the penalty by adding additional PCM.

5. An HTeDP Integrated with TMS with Eutectic Compound PCM as the Solution for Peak Thermal Load (PCM2)

This case incorporates a type of eutectic compound PCM, Urea-KCL, as the solution to absorb the heat that cannot be removed. Similarly, a thermal management analysis will be conducted to show the cooling capability of this type of PCM. The assessment of the block fuel burn performance will also be conducted to show in the impact by installation of the PCM.

V. Results and Analysis

In this section, the thermal management analyses for the 5 cases, Baseline, BaseTMS, AddPAO, PCM1, and PCM2, are firstly presented, from Sec. V. A to Sec. V. E. Then the system-level and mission-level impacts of the TMS for all the cases are assessed and compared in Sec. V. F. As mentioned before, the 600-nmi-range and 8,100-lb-payload mission is selected for the thermal management analysis, and missions with different ranges and payloads are selected in assessment of the TMS impacts at system and mission level.

A. Heat Generation Analysis for Baseline Case without TMS

The heat generation of a single IMD (8 IMD in total for the whole ULI aircraft) for the baseline case through the selected off-design mission is illustrated in Fig. 10. The peak heat generation rate of a single IMD is 108.7 kW during takeoff, and the total generated heat of a single IMD is 134.7 MJ. Thus, the peak heat generation rate of the whole aircraft is 869.6 kW and the total heat generation is 1077.6 MJ through the mission. Considering the existing More-Electric Aircraft, Boeing 787, of which the electrical load greatly increases compared to traditional commercial aircraft due to electrification of subsystems, its total electrical load is 944 kW with an efficiency from 80% to 97% [26], so the corresponding maximum possible heat generation rate is around 188 kW, which is much smaller than the heat

generation rate of the IMD of the ULI aircraft. Therefore, traditional TMS for electrical systems may not be capable of handling the heat removal problem of an HTeDP aircraft. A thorough study must be conducted on the design and analysis of the TMS to validate if its cooling capability is sufficient to handle such high heat generation.
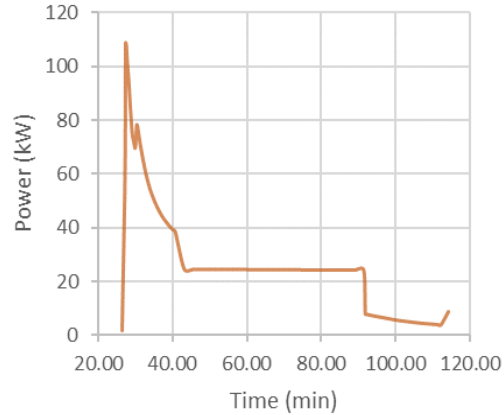

Fig. 10 Heat generation of a single IMD for the Baseline case through the selected mission

B. Thermal Management Analysis for Case BaseTMS (basic TMS without heat absorption)

The removed heat and generated heat for the BaseTMS case are compared in this section, where the TMS does not include the solution for the peak thermal load. The 600-nmi-range and 8,100-lb-payload off-design mission is selected for this thermal analysis as mentioned before. The TMS is sized at the takeoff (TKO) condition with a standard international atmosphere (ISA), where the flight altitude is 0 ft, and the Mach number is 0.3. The performance of the TMS is influenced by the sizing condition of the ACOC and the upper limit of the fraction of fan cooling bleed to the core flow (Bleed_limit). The sizing variable for the ACOC is the air side pressure drop (dP_air). It should be noted that the design effectiveness can be determined by the design pressure drop, and vice versa. The bleed limit works in the following way: the amount of the extracted cooling bleed is adjusted to cool the PAO to the target temperature through a numerical solver, but if the bleed hits its upper limit while the target temperature is still not matched, then the amount of the bleed is set to the upper limit, leaving the PAO not fully cooled. In this study, the design pressure drop is selected as the sizing variable. The results of the TMS with dP_air=0.01, and Bleed_limit=0.05 is presented first. Then a sensitivity analysis against different air side pressure drop and bleed extraction limitation.

1. TMS Results with Sizing dP_air=0.01 and Bleed_limit=0.05

The heat removal and the heat generation for a single IMD TMS through the whole mission are plotted together in Fig. 11(a), and the difference between the generation and the removal is illustrated in Fig. 11(b). Compared to case Baseline, of which the corresponding heat generation is illustrated in Fig. 10, heat can be removed using the basic TMS for most segments of the mission. However, it can be discovered that there is a gap during the early mission segment, where it is the takeoff and early segment of climb. This gap is caused by two major reasons. The first one is that the cooling capability of the fan bleed is the lowest through the mission during takeoff and climb, because the air temperature is high at low altitudes. The second one is that the power of the motor is the highest during these mission segments since the power requirement is the highest during takeoff and climb. A secondary reason is that the heat exchanger effectiveness during the takeoff and climb is low, which is shown in Fig. 12. This secondary reason also caused by the previous two major reasons: air temperature is high which reduces the temperature difference between the air and PAO; and the motor power is high which increases the required amount of the cooling bleed, reducing the number of transfer units (NTU), leading to a low effectiveness. As shown in Fig. 12, as the altitude goes up (may refer to Fig. 9 to see the corresponding flight altitude for certain timestamps), the effectiveness also increases because of lower air temperature and higher NTU. The total heat that cannot be removed is 5092.58 kJ for a single IMD, which is obtained through integral of power difference over the mission time. Therefore, a solution is needed to handle the peak thermal load during early mission segments for the TMS with current sizing condition. However, before implementing any of the heat absorption solutions for this problem, different sizing conditions and settings need to be investigated first. Thus, a sensitivity analysis is performed against different sizing air side pressure drop and cooling bleed limitation to test if varying such conditions can solve this problem.
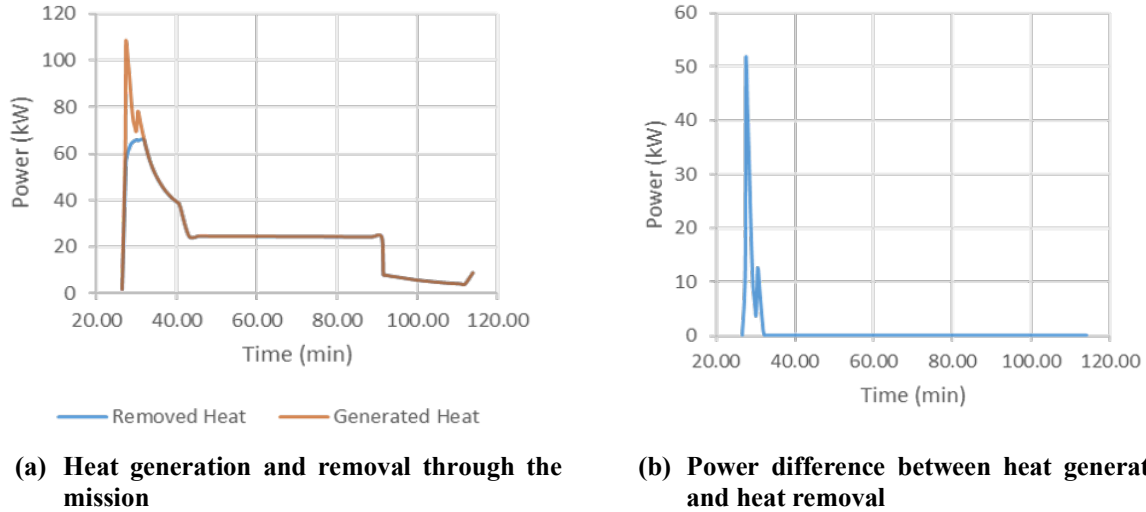
13

(a) **Heat generation and removal through the mission**

(b) **Power difference between heat generation and heat removal**

Fig. 11 Thermal management performance of a single IMD TMS for case BaseTMS with sizing dP_air=0.01, Bleed_limit=0.05
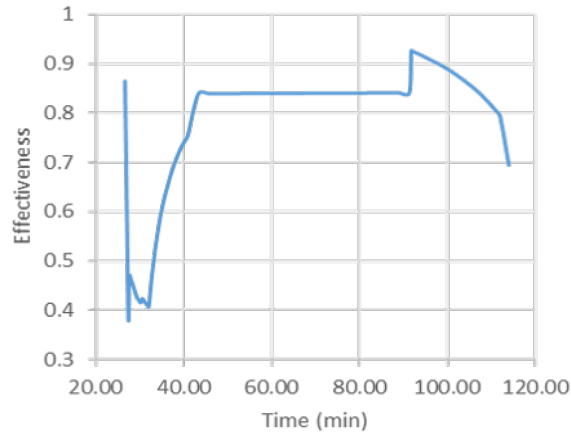

Fig. 12 ACOC effectiveness for case BaseTMS through the mission with sizing dP_air=0.01, Bleed_limit=0.05

2. Sensitivity Analysis against Sizing dP_air

The removed heat and generated heat of the TMS for a single IMD TMS against different sizing air side pressure drop are illustrated in Fig. 13(a), and the corresponding power difference is shown in Fig. 13(b). In this sensitivity analysis, sizing dP_air =0.005, 0.01, 0.02, 0.03, 0.04 while keeping Bleed_limit=0.05. It is discovered that as sizing dP_air increases, more heat can be removed while the heat generation is almost the same for all cases. This is because as sizing dP_air increases, the effectiveness of ACOC increases, as shown in Fig. 14. It should be noted that although the effectiveness of the case with higher sizing dP_air is higher through the whole mission, the heat generated during cruise or descent can be fully removed for all the cases. This is because the cooling bleed is not limited by the bleed fraction limit, meaning that more cooling bleed can be used to cool the PAO in cases with lower effectiveness. The corresponding mass flow rate of the bleed air for a single IMD TMS can be seen in Fig. 15. During early mission segments, the required bleed air hits the upper limit for all cases, therefore, the curves are overlapped for the first several minutes. As this bleed air constraint becomes inactive, it can be found that the required mass flow rate of the bleed becomes less as the sizing dP_air increases. On the other hand, increasing sizing dP_air becomes less effective when dP_air is high. For example, the difference between heat removal curves of dP_air=0.01 and dP_air=0.02 is significant while heat removal curves of dP_air=0.03 and dP_air=0.04 almost overlap each other, as shown in Fig. 13(a). The heat that cannot be removed through the whole mission for a single IMD against different sizing dP_air is presented in Fig. 16, which indicates that increasing dP_air does help to remove more heat, however, as dP_air increases such approach becomes very limited. Moreover, dP_air cannot be increased as much as wanted, because the

14

pressure drop is constrained by the heat exchanger volume. Therefore, increasing dP_air cannot solve the problem of the heat removal.
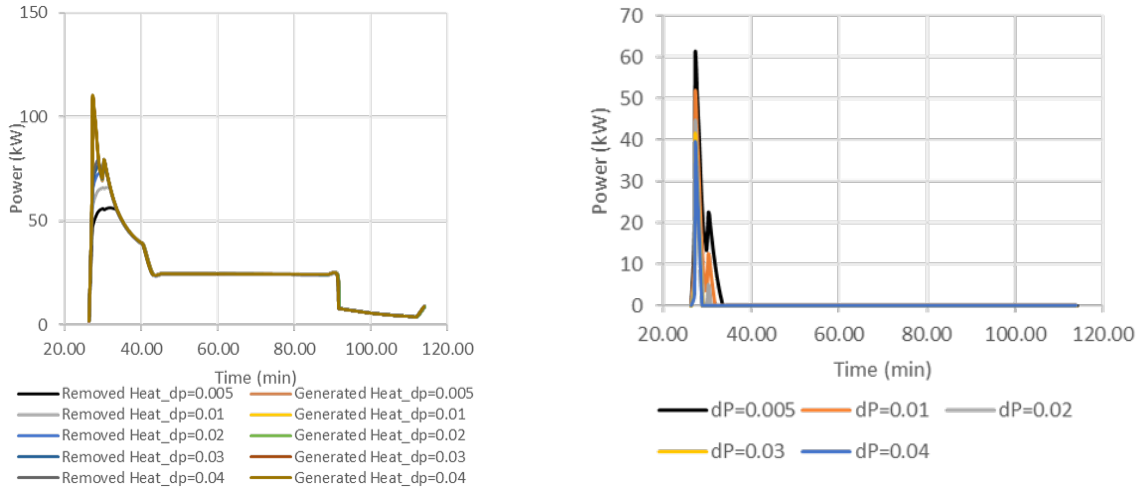
(a) Heat generation and removal through the mission with different sizing dP_air, while Bleed_limit=0.05

(b) Power difference between heat generation and removal with different sizing dP_air, while Bleed_limit=0.05

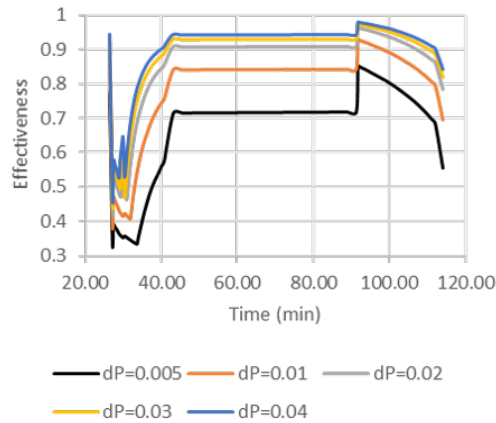**Fig. 13 Thermal management performance of a single IMD TMS for case BaseTMS with different sizing dP_air, while Bleed_limit=0.05**

Fig. 14 ACOC effectiveness with different sizing dP_air, while Bleed_limit=0.05
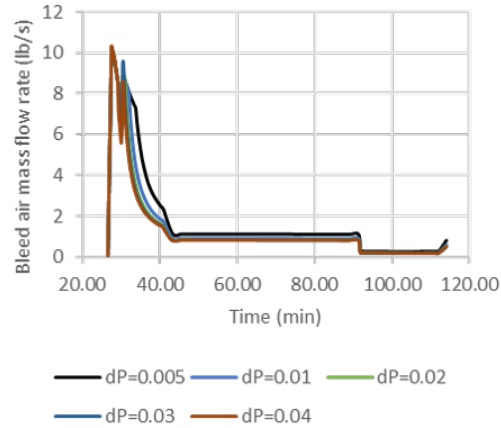
Fig. 15 Cooling bleed mass flow rate for a single IMD TMS with different sizing dP_air, while Bleed_limit=0.05
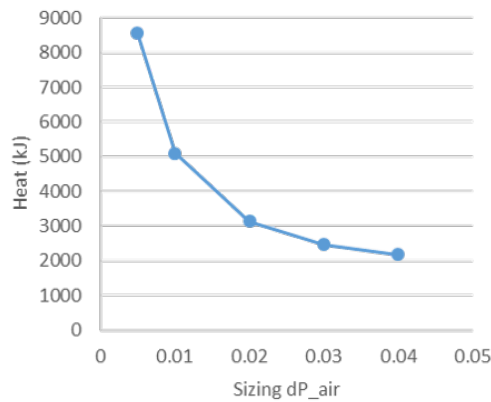
Fig. 16 Heat cannot be removed for a single IMD with different sizing dP_air, while Bleed_limit=0.05

3. Sensitivity Analysis against Bleed_limit

In this sensitivity analysis, different Bleed_limit is used to test the performance of the TMS, while keeping dP_air=0.01. Bleed_limit=0.03, 0.04, 0.05, 0.06 ,0.07 are selected to perform this analysis. The removed and generated heat through the mission for a single IMD TMS are shown in Fig. 17(a), and the corresponding power difference is illustrated in Fig. 17(b). The total heat that cannot be removed is plotted in Fig. 18. From these figures, it can be concluded that as Bleed_limit increases from 0.03 to 0.05, more heat can be removed, but as Bleed_limit increases from 0.05 to 0.07 the removed heat is reduced. This is because increasing the cooling bleed upper limit can improve the cooling capacity of the cold air flow while reducing the effectiveness of the ACOC. The cooling capacity is increased because of more cold air flow passes through the heat exchanger. However, more mass flow also degrades the performance of the ACOC, which is presented in Fig. 19. Thus, these two facts counter the effect of each other on the performance of the TMS. From Bleed_limit=0.03 to 0.05, the increase of cooling capacity is dominant, while from Bleed_limit=0.05 to 0.07 the degradation of effectiveness is more dominant, leading to the fact that the maximum heat will be removed when Bleed_limit is around 0.05. Therefore, varying the fan bleed extraction upper limit cannot solve the heating problem during takeoff and climb.
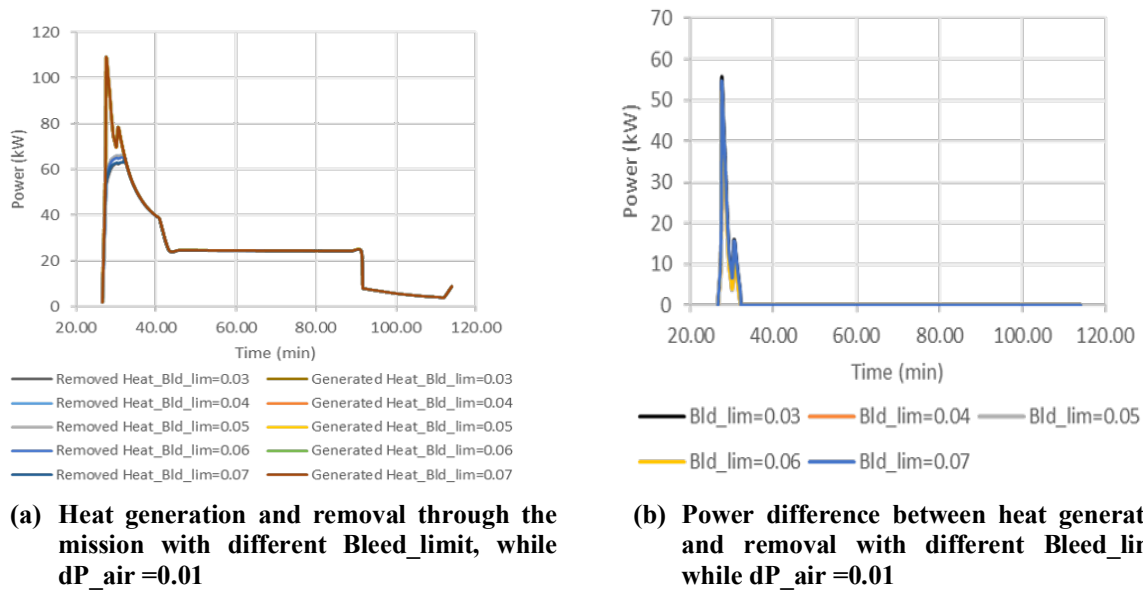
(a) **Heat generation and removal through the mission with different Bleed_limit, while dP_air =0.01**

(b) **Power difference between heat generation and removal with different Bleed_limit, while dP_air =0.01**

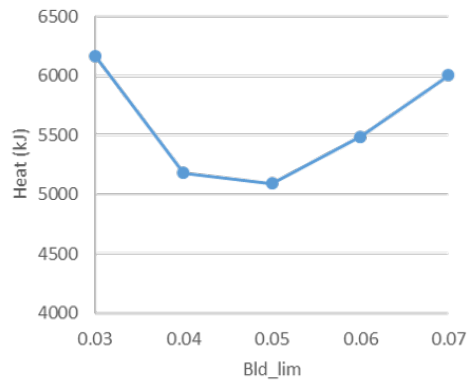**Fig. 17 Thermal management performance of a single IMD for case BaseTMS with different Bleed_limit, while dP_air =0.01**

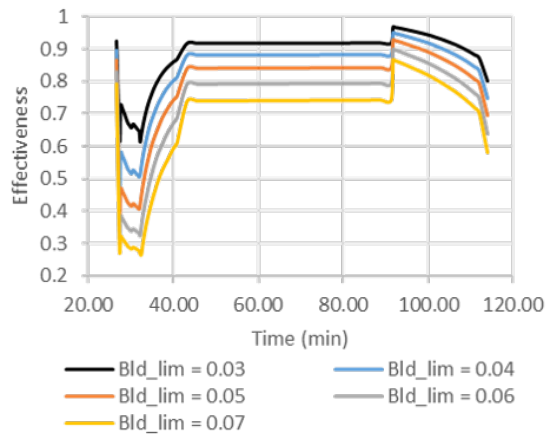**Fig. 18 Heat cannot be removed for a single IMD with different Bleed_limit, while dP_air =0.01**

Fig. 19 ACOC effectiveness with different Bleed_limit, while dP_air =0.01

17

C. Thermal Management Analysis for Case AddPAO (TMS with additional PAO for heat absorption)

As discussed in the previous sections, varying TMS sizing conditions and settings cannot solve the heating problem during the early mission segments. Therefore, solutions incorporating certain media to absorb the heat during early segments are studied. In this section, the thermal management performance of the TMS with additional PAO as the heat absorption is assessed. The basic TMS is still sized with dP_air=0.01, and Bleed_lim=0.05. The corresponding heat generation and removal for a single IMD TMS is illustrated in Fig. 20(a), and the heat removal distribution among the basic TMS and additional PAO is shown in Fig. 20(b). It is seen that the two curves representing heat generation and removal overlap each other, meaning that the heat generation is equal to the heat removal through the whole mission, indicating that the additional PAO solution is capable of handling the heating problem during early mission segments. Compared to Fig. 11(a) and Fig. 11(b), the heat removal distribution in Fig. 20(b) shows that the heat absorbed by the basic TMS is still the same and only the part of heat that cannot be removed is absorbed by the additional PAO. The required mass flow rate of the additional PAO is illustrated in Fig. 21, which is proportional to the heat absorbed by the additional PAO as in Fig. 20(b).
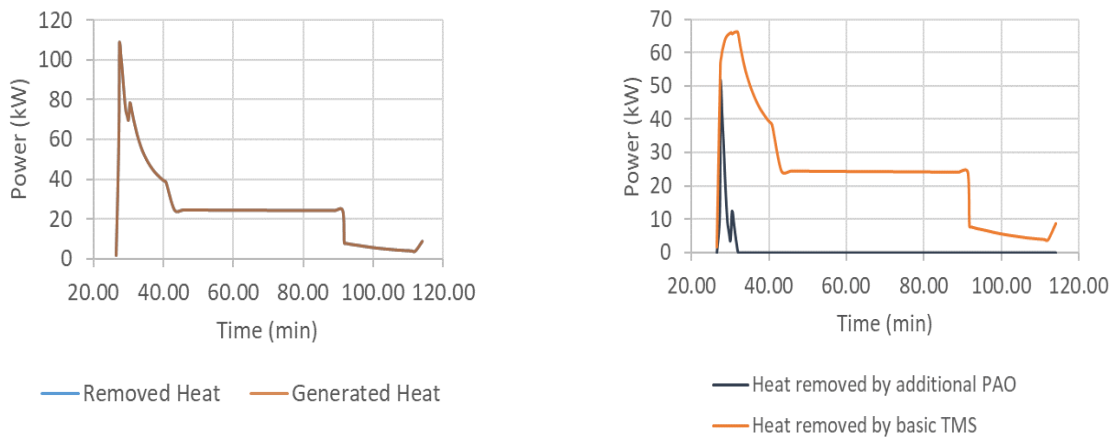
(a) Heat generation and removal through the mission using additional PAO

(b) Heat removal distribution among the basic TMS and additional PAO

Fig. 20 Thermal management performance of a single IMD TMS using additional PAO as heat absorption
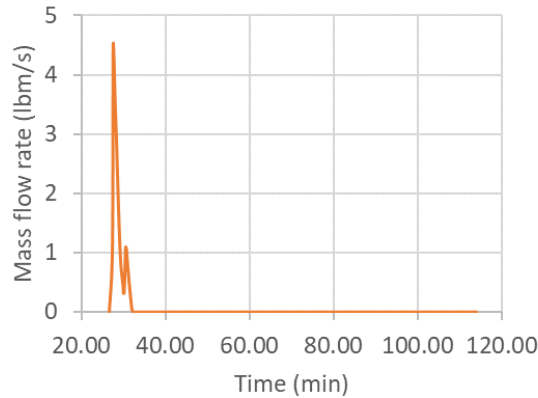

Fig. 21 Required mass flow rate of the additional PAO for a single IMD TMS

D. Thermal Management Analysis for Case PCM1 and PCM2 (TMS with two types of PCM for heat absorption)

The thermal analysis of the heat absorption solution that incorporates PCM is discussed in this section. The heat generation and removal for case PCM1 which uses magnesium chloride hexahydrate is presented in Fig. 22(a), and the corresponding heat removal distribution among the PCM and the basic TMS is illustrated in Fig. 22(b). The heat

generation and removal for case PCM2 which uses Urea-KCL is presented in Fig. 23(a), and the corresponding heat removal distribution among the PCM and the basic TMS is illustrated in Fig. 23(b). It is seen that the solution using either magnesium chloride hexahydrate or Urea-KCL can satisfy the cooling requirement during early mission segments because the heat removal equals the heat generation as shown in Fig. 22(a) and Fig. 23(a). However, the behavior of heat removal distribution by using PCM is quite different from the solution using additional PAO, which can be discovered by comparing Fig. 22(b) and Fig. 23(b) with Fig. 20(b). The heat absorption rate of the PCM reaches the maximum at the beginning when all the PCM is in the solid state. As the melting process goes on, the heat absorption rate slight goes down, and after the PCM is fully melted, the heat absorption rate drops quickly to zero when the PCM reaches the temperature of the stator temperature. In contrast to Fig. 20(b) in which the additional PAO only absorbs the excessive heat, the PCM absorbs more than the heat that cannot be removed by the basic TMS, making the heat removed by the basic TMS less than that in case BaseTMS or AddPAO. The difference in distribution of removed heat between solution with additional PAO and solution with PCM can be explained by the fact that the mass flow rate of the additional PAO can be adjusted to only absorb the amount of heat that cannot be removed, but for the PCM, its heat transfer rate cannot be controlled once the size is determined. By comparing Fig. 22(b) and Fig. 23(b), it is also found that the heat transfer rate by using Urea-KCL is higher than using magnesium chloride hexahydrate because Urea-KCL has a higher thermal conductivity.
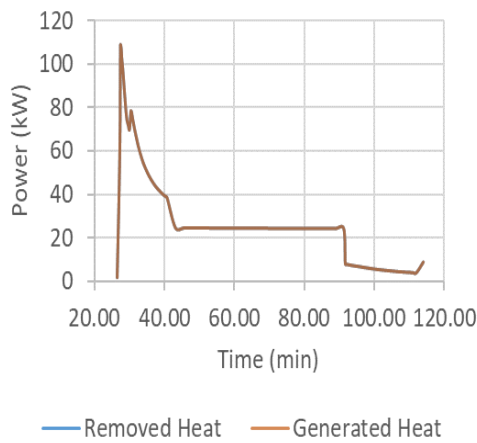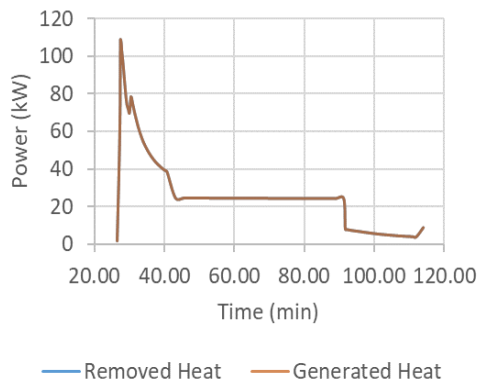

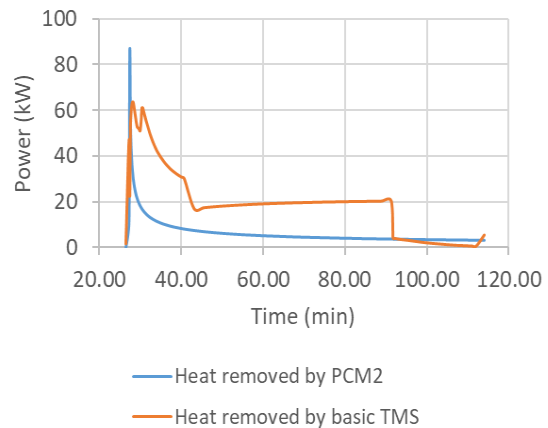(a) **Heat generation and removal through the mission using PCM1**
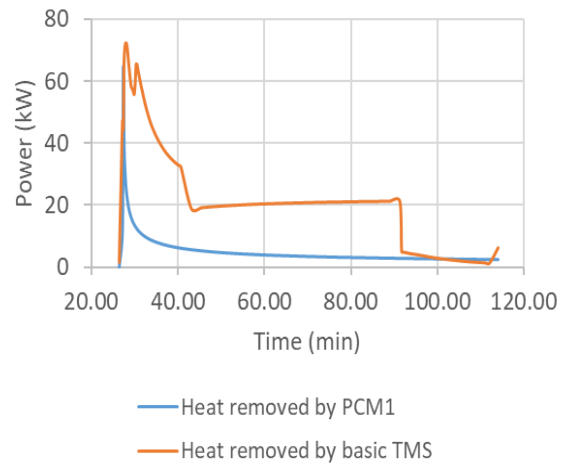
(b) **Heat removal distribution among the basic TMS and PCM1**

Fig. 22 Thermal management performance of a single IMD TMS with magnesium chloride hexahydrate as heat absorption

(a) **Heat generation and removal through the mission using PCM2**

(b) **Heat removal distribution among the basic TMS and PCM2**

Fig. 23 Thermal management performance of a single IMD TMS using Urea-KCL as heat absorption

E. Impacts of TMS at the System and Mission level

1. Impacts of TMS on Weight

The major penalty brought by the TMS is the additional weight. The direct weight penalty (for 8 IMD) of each type of TMS, which is the weight added by the TMS component, coolant, and heat absorption media, is illustrated in Fig. 24. It is discovered that the TMS with additional PAO (AddPAO) has the largest component weight increase from the BaseTMS, while the two cases with PCM only add relatively small amount of weight. Although the heat absorbed by TMS with additional PAO or PCM is the same, the high latent heat of the two types of PCM make the required weight much smaller. Comparing case PCM1 and PCM2, the TMS using Urea-KCL is slightly lighter than TMS using magnesium chloride hexahydrate because the latent heat of Urea-KCL is higher while the melting temperatures of them are almost the same. It should be also noted that the weight of the TMS can lead to upsizing of other aircraft systems which will result in a larger weight increase than the weight only added by the TMS. For example, as the weight of the TMS is added to the aircraft, the propulsion system needs to be upsized to provide more thrust, and the upsizing of the engine increases the weight of the aircraft as well. The takeoff weight of the aircraft with different TMS are presented in Fig. 25, which is normalized by the takeoff weight of the baseline case. The impacts on takeoff weight includes both the pure weight of the TMS and the upsizing influences. The takeoff weight increases by all the types of TMS, which are 1.64% (BaseTMS), 9.17% (AddPAO), 4.06% (PCM1), and 3.76% (PCM2), are not trivial. Thus, the impacts of TMS at the aircraft or mission level cannot be neglected, although many existing literatures did not consider such impacts in assessment of electrical propulsion configurations. Consistent with the pure weight added by TMS, the aircraft with TMS using additional PAO has the largest takeoff weight, while the takeoff weight of the aircraft with TMS using PCM only increases a small amount compared to the case AddPAO. Therefore, for the TMS that can handle the early mission heating problem, which all use heat absorption, the TMS with Urea-KCL has the best performance in terms of the penalty weight while the TMS with additional PAO has the largest weight increase.
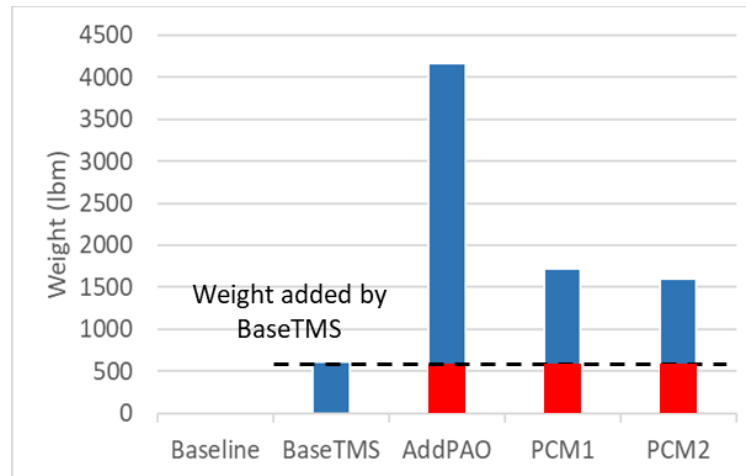

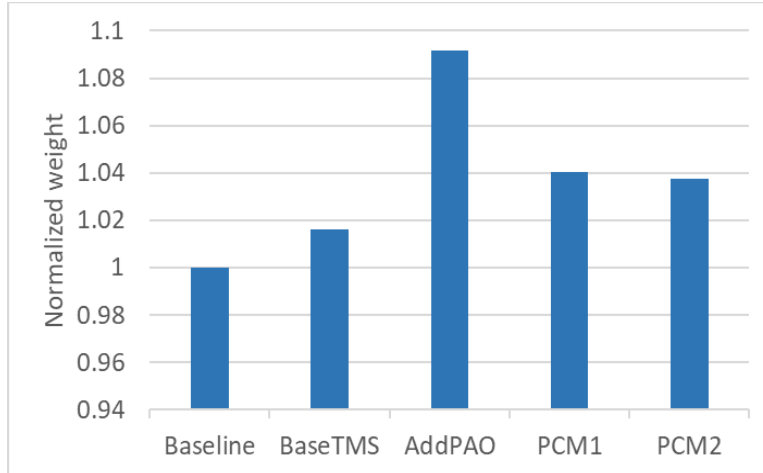**Fig. 24 Direct penalty weight added by each type of TMS**

Fig. 25 MTOW of ULI aircraft with each type of TMS

2. Impacts of TMS on Mission Block Fuel Burn

As mentioned in Sec. IV. B, missions with different ranges and payloads are selected for the block fuel burn analysis, where the normalized range (normalized by the design range) is from 0.1 to 0.6 and the normalized payload (normalized by the design payload)is from 0.1 to 0.6. The reason to select short-rang and low-payload missions is that the ULI program focuses on hybridization of the aircraft by installation of battery for such short-rang and low-payload missions to improve the fuel burn performance, which has been also discussed in Sec. IV. B. The increases of block fuel burn among the selected missions of case BaseTMS, AddPAO, PCM1, and PCM2 relative to case Baseline are shown Fig. 26. From these figures, it can be discovered that the BaseTMS has the lowest increase of the block fuel burn (around 1% to 1.3%) compared to the baseline case no TMS is installed, and the TMS with additional PAO has the highest fuel penalty (around 6.5% to 9%), while the performances of case PCM1 (around 2.8% to 3.8%) and PCM2 (around 2.7% to 3.5%) are in between and PCM2 is slightly better than PCM1. Such phenomenon is associated with the penalties on the takeoff weight of the aircraft as shown in Fig. 25. It is also found that as range increases, the penalty of the TMS on block fuel burn increases. This is because the major penalty of installation of TMS is the additional weight, and as the flight distance increases, more fuel is needed to carry such added weight. It is also seen that at a fixed mission range, the relative increase of the block fuel burn is almost kept the same. This is because the additional fuel weight to carry the TMS is unchanged as the payload varies, leading to the fact that the fuel burn penalty due to TMS is insensitive to payload. In summary, among the TMS that can sufficiently cool the IMD during early mission segments, the one with Urea-KCL (PCM2) has the best fuel economy.
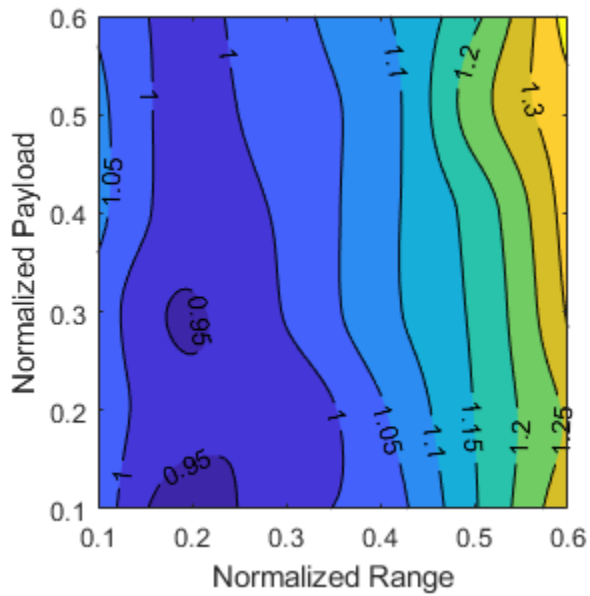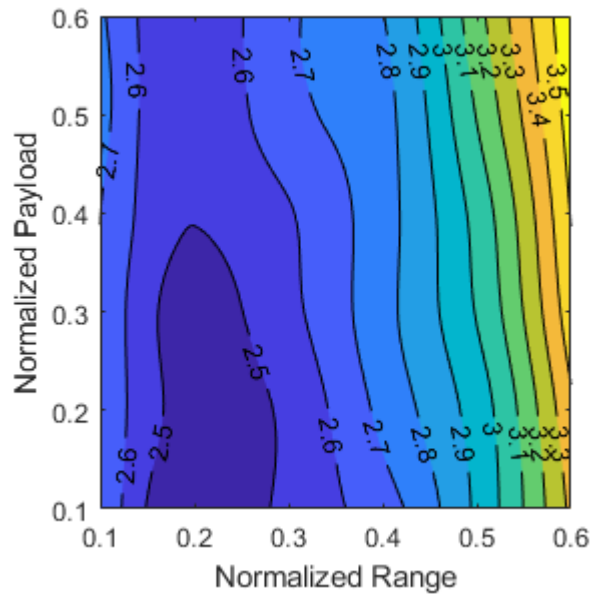
(a) **Relative block fuel burn increase of BaseTMS to Baseline**
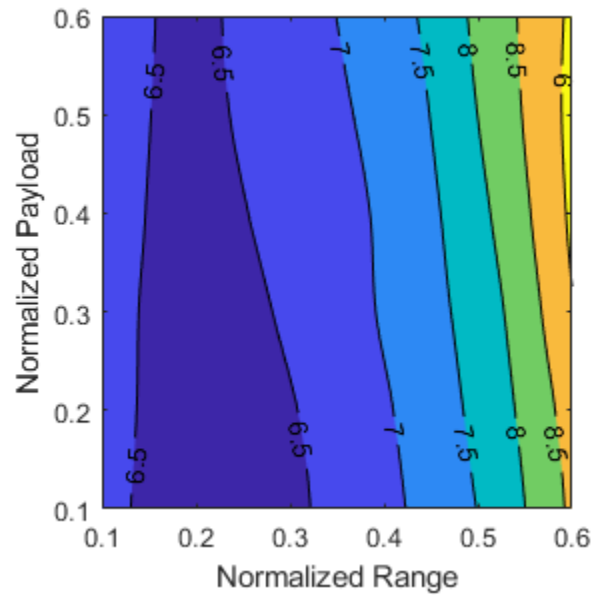
(b) **Relative block fuel burn increase of AddPAO to Baseline**
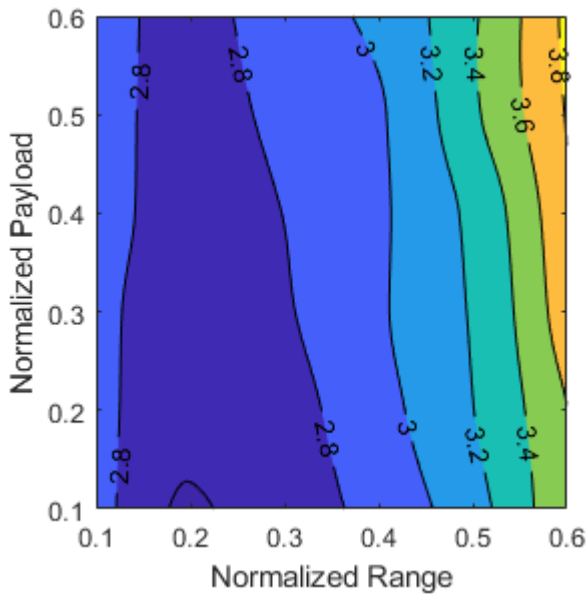
(c) **Relative block fuel burn increase of to Baseline**

(d) **Relative block fuel burn increase of PCM2 to Baseline**

Fig. 26 Relative increase of block fuel burn of aircraft with each TMS to the baseline for different normalized payloads and ranges (%)

VI. Conclusions and Future Work

This paper fills the gap that many existing literatures neglected the thermal management system when analyzing the electrical propulsion configurations, by integrating the thermal management system to the aircraft model as well as conducting assessment its cooling capability as well as the system- and mission-level impacts. Firstly, following the assumption made by many works that the TMS can be neglected, a heat generation analysis of the baseline aircraft without TMS showed that a great amount of heat is generated from the electrical propulsion system through the whole

mission, which is much greater than the heat generated from electrical systems in existing commercial aircraft, making the heating problem non-trivial. Then a traditional air-oil TMS was integrated to the vehicle model and the corresponding cooling capacity was analyzed. However, it was found that the peak thermal load during early mission segments cannot be fully removed by this TMS. Therefore, three architectures of TMS with media to absorb the excessive heat were proposed: one with additional PAO as the heat absorption, and two others with two types of PCM (magnesium chloride hexahydrate and Urea-KCL). The thermal analyses of these three TMS showed that all of them can sufficiently cool the electrical propulsion system. The impacts of the basic TMS and TMS with heat absorption media on the aircraft and the missions are also assessed, showing that non-negligible penalties on the aircraft MTOW and mission block fuel burn were added by all these four TMS architectures. The TMS with additional PAO has the largest penalties on weight and block fuel burn, while the corresponding penalties of TMS with PCM are much smaller because the large latent heat of the PCM makes it much lighter than PAO. Comparing the TMS with two types of PCM, the penalty added by Urea-KCL is slightly smaller than that by magnesium chloride hexahydrate because Urea-KCL has larger latent heat and thermal conductivity. From the observations above, it can be concluded here that a thermal analysis must be conducted on the TMS for the novel electrical propulsion system to ensure sufficient cooling capability because traditional TMS may not be able to handle the great amount of the generated heat. Solutions using heat absorption media is demonstrated to be able to effectively manage the peak thermal load during early mission segments, while weight penalties due to heat absorption materials is added. To absorb the same amount of heat, PCM is also shown to be lighter than the cooling oil because of the high latent heat.

In the future, the authors will investigate more TMS architectures for the cooling requirement of the propulsion system of HTeDP aircraft and try to formulate a methodology to generate an optimal architecture in terms of selected performance metrics of interest. On the other hand, a higher-fidelity analysis of the PCM may be needed to further validate the design decision of the TMS using PCM.

Acknowledgments

References

[1] Wahls, R., "N+3 Technologies and Concepts," online: http://www.aeronautics.nasa.gov/pdf/wahls_2_green_aviation_summit.pdf, accessed Oct. 21, 2017.

[2] Greener by Design Executive Committee, "Air Travel - Greener By Design Anuual Report 2015-2016," online: https://www.aerosociety.com/media/4013/2016_gbd_report_web.pdf, accessed Oct. 21, 2017.

[3] Perullo, C., Alahmad, A., Wen, J., D'Arpino, M., Canova, M., Mavris, D. N., and Benzakein, M. J. "Sizing and Performance Analysis of a Turbo-Hybrid-Electric Regional Jet for the NASA ULI Program". In AIAA Propulsion and Energy 2019 Forum (AIAA 2019-4490).
Doi: 10.2514/6.2019-4490

[4] Perullo, C., Shi, M., Cinar, G., Alahmad, A., Sanders, M., Mavris, D. N., and Benzakein, M. J., "An Update on Sizing and Performance Analysis of a Hybrid Turboelectric Regional Jet for the NASA ULI Program", In AIAA/IEEE Electric Aircraft Technologies Symposium 2020.

[5] Felder, J., Kim, H., and Brown, G., "Turboelectric Distributed Propulsion Engine Cycle Analysis for Hybrid-Wing-Body Aircraft," 47th AIAA Aerospace Sciences Meeting including The New Horizons Forum and Aerospace Exposition, 2008, (AIAA 2009-1132).
Doi: 10.2514/6.2009-1132

[6] Felder, J., Kim, H., Brown, G., and Kummer, J., "An examination of the effect of boundary layer ingestion on turboelectric distributed propulsion systems,"49th AIAA aerospace sciences meeting including the new horizons forum and aerospace exposition, 2011, (AIAA 2011-300).
Doi: 10.2514/6.2011-300

[7] Liu, C., Doulgeris, G., Laskaridis, P., and Singh, R., "Thermal cycle analysis of turboelectric distributed propulsion system with boundary layer ingestion," Aerospace Science and Technology, Vol. 27, No. 1, 2013, pp. 163–170.
Doi: 10.1016/j.ast.2012.08.003

[8] Welstead, J. and Felder, J. L., "Conceptual design of a single-aisle turboelectric commercial transport with fuselage boundary layer ingestion,"54th AIAA Aerospace Sciences Meeting, 2016 (AIAA 2016–1027).
Doi: 10.2514/6.2016-1027

[9] Shi, M., Pokhrel, M., Gladin, J. C., Garcia, E., and Mavris, D. N., "Model Fidelity Requirements in Boundary Layer Ingestion Propulsion System Conceptual Design,"18th AIAA Aviation Technology, Integration, and Operations Conference, AIAA AVIATION Forum, 2018 (AIAA 2018-3835).
Doi: 10.2514/6.2018-3835.

[10] Shi, M., Pokhrel, M., Gladin, J. C., Garcia, E., and Mavris, D. N., "Modeling Fidelity Requirements of Mission-Level Analysis on Boundary Layer Ingestion Propulsion System," AIAA Scitech 2019 Forum, 2019 (AIAA 2019-1590).
Doi: 10.2514/6.2019-1590

[11] Shi, M., Pokhrel, M., Gladin, J. C., and Mavris, D. N., "Conceptual Design of a BLI Propulsor Capturing Aero-Propulsive Coupling and Distortion Impacts," AIAA Scitech 2019 Forum, 2019 (AIAA 2019-1588).
Doi: 10.2514/6.2019-1588

[12] McCluskey, P., Saadon, Y., Yao, Z., Shah, J., & Kizito, J., "Thermal Management Challenges in Turbo-Electric and Hybrid Electric Propulsion". In 2018 International Energy Conversion Engineering Conference 2018 (AIAA 2018-4695).
Doi: 10.2514/6.2018-4695

[13] R. Kabir, K. Kaddoura, F. P. McCluskey and J. P. Kizito, "Investigation of a Cooling System for A Hybrid Airplane," 2018 AIAA/IEEE Electric Aircraft Technologies Symposium (EATS), Cincinnati, OH, 2018, pp. 1-18.

[14] Rheaume, J., & Lents, C. E., "Design and simulation of a commercial hybrid electric aircraft thermal management system," In 2018 AIAA/IEEE Electric Aircraft Technologies Symposium (AIAA 2018-4994).
Doi: 10.2514/6.2018-4994

[15] Perullo, C., Tai, J., and Mavris, D., "A New Sizing and Synthesis Environment for the Design and Assessment of Advanced Hybrid and Electric Aircraft Propulsion Systems," International Association of Airbreathing Engines (ISABE), 2015 (ISABE-2015-20286).
Doi: 2374.UC/745831

[16] Sharma, A., Tyagi, V. V., Chen, C. R., & Buddhi, D., "Review on thermal energy storage with phase change materials and applications," Renewable and Sustainable energy reviews, 13(2), 318-345.
Doi: 10.1016/j.rser.2007.10.005

[17] Gladin, J. C., Perullo, C., Tai, J. C., and Mavris, D. N., "A Parametric Study of Hybrid Electric Gas Turbine Propulsion as a Function of Aircraft Size Class and Technology Level,"55th AIAA Aerospace Sciences Meeting, 2017, (AIAA 2017-0338).
Doi: 10.2514/6.2017-0338

[18] Gladin, J., Trawick, D., Perullo, C., Tai, J. C., and Mavris, D. N., "Modeling and Design of a Partially Electric Distributed Aircraft Propulsion System with GT-HEAT,"55th AIAA Aerospace Sciences Meeting, 2017 (AIAA 2017-1924).
Doi: 10.2514/6.2017-1924

[19] Claus, R., Evans, A., & Follen, G., "Multidisciplinary propulsion simulation using NPSS. In 4th Symposium on Multidisciplinary Analysis and Optimization," 1992 (p. 4709).
Doi: 10.2514/6.1992-4709

[20] Kays, W. M. and London, A. L.,Compact heat exchangers, McGraw-Hill, New York, NY, 1984.

[21] Shi, M., Chakraborty, I., Tai, J. C., and Mavris, D. N., "Integrated Gas Turbine and Environmental Control System Pack Sizing and Analysis,"2018 AIAA Aerospace Sciences Meeting, (AIAA 2018-1748), 2018.
Doi: 10.2514/6.2018-1748

[22] "Air Carrier Statistics Database (T-100)," DOE Bureau of Transportation Statistics, 2013. [Online].

[23] Jankowski, Nicholas R., and F. Patrick McCluskey. "A review of phase change materials for vehicle component thermal buffering." Applied Energy 113 (2014): 1525-1561.
Doi: 10.1016/j.apenergy.2013.08.026

[24] Hewitt, Neil J. "Heat pumps and energy storage–The challenges of implementation." Applied Energy 89.1 (2012): 37-44.
Doi: 10.1016/j.apenergy.2010.12.028

[25] Mansouri, Larbi, Mourad Balistrou, and Bernard Baudoin. "One-dimensional time-dependent modeling of conductive heat transfer during the melting of an initially subcooled semi-infinite PCM." Congrès français de mécanique. AFM, Association Française de Mécanique, 2017.
URI: 2042/63169

[26] Whyatt, Greg A., and Lawrence A. Chick. "Electrical generation for more-electric aircraft using solid oxide fuel cells". No. PNNL-21382. Pacific Northwest National Lab. (PNNL), Richland, WA (United States), 2012.